Lipopolysaccharide-induced glycolytic reprogramming drives H3K18 lactylation-mediated inflammatory injury in buffalo mammary epithelial cells

Peng Xiao[1,2,3,4], Xin-Ru Tian[1,2,3], Jin-Chen Zhou[2,3], Bo Zhang[1], Meng-Qi Li[1,2,3], Chun-Yan Yang[2,3], Hai-Ying Zheng[2,3], Meng-Jiao Chen[4], Xiao-Gan Yang[1], Jiang-Hua Shang[2,3]*, Xing-Wei Liang[1]*

[1] *Guangxi Key Laboratory of Animal Breeding, Disease Control and Prevention, College of Animal Science & Technology, Guangxi University, Nanning, Guangxi,* 530004*, China.*

[2] *Guangxi Key Laboratory of Buffalo Genetics, Reproduction and Breeding, Guangxi Buffalo Research Institute, Chinese Academy of Agricultural Sciences, Nanning* 530001*, China.*

[3] *Key Laboratory of Buffalo Genetics, Breeding and Reproduction Technology, Ministry of Agriculture and Rural Affairs, Nanning* 530001*, China.*

[4] *College of Animal Science and Technology, Guangxi Vocational University of Agriculture, Nanning,* 530007*, China.*

*Corresponding author: Xing-Wei Liang (xwliang@gxu.edu.cn) and Jiang-Hua Shang (jh_shang@163.com)

Science Press

ZR Zoological Research

ABSTRACT

Buffalo mastitis impairs milk production and quality, yet the underlying epigenetic mechanisms remain unclear. While LPS-induced glycolytic activation and lactate accumulation contribute to inflammation, their role in histone lactylation-mediated injury is unexplored. Our results revealed that mammary tissues from buffalo with clinical mastitis exhibited elevated LPS levels, upregulation of inflammatory markers, enhanced apoptosis, and markedly higher levels of lactate, Pankla, and H3K18la compared to healthy controls. Similarly, an LPS-induced mouse mastitis model recapitulated the inflammatory and apoptotic features observed in buffalo tissues, confirming LPS as a key driver of mammary tissue injury. In vitro, LPS treatment of buffalo mammary epithelial cells (BuMECs) upregulated proinflammatory and proapoptotic markers while downregulating antiapoptotic genes. RNA-seq and western blot analyses further revealed that LPS enhanced the expression and activity of key glycolytic enzymes, such as *HK2*, *PKM2*, *PDK1*, and *LDHA*, thereby promoting glycolytic flux, increasing lactate production, and elevating Pankla and H3K18la levels. CUT&Tag analysis suggested that H3K18la may facilitate the recruitment of transcriptional regulators, such as *DDIT3*, *NF-κB1*, and *CEBPD*, potentially linking lactylation to the activation of inflammatory and apoptotic pathways. Importantly, inhibition of *HK2* reduced lactate accumulation, decreased H3K18la levels, and substantially attenuated inflammatory injury in BuMECs. Together, these findings identify the HK2-lactate-H3K18la axis as a central mechanism in LPS-induced inflammatory injury in BuMECs and underscore its potential as a therapeutic target for alleviating mastitis and enhancing mammary health in dairy buffalo.

Key words: Lipopolysaccharide; Mastitis; Buffalo mammary epithelial cells; Glycolysis; Histone lactylation

INTRODUCTION

Mastitis is a highly prevalent and economically significant disease in the global dairy industry, substantially limiting buffalo milk production and compromising dairy safety. Its pathogenesis is primarily driven by inflammatory responses triggered by bacterial invasion of mammary tissue (Ali et al., 2021). Clinical mastitis can reduce daily milk yield in buffalo by up to 50%, whereas subclinical mastitis, often presenting without overt symptoms, results in production losses of 5-15%, imposing significant economic burdens on farmers reliant on buffalo milk (Costa et al., 2020). Elevated somatic cell counts (SCC) in infected udders disrupt casein synthesis, leading to 18-22% reductions in milk fat content, 0.23-0.35% decreases in lactose levels, and abnormal elevations of sodium and chloride ions, which disrupt osmotic balance and negatively affect milk flavor (Patbandha et al., 2015; Puggioni et al., 2020). Additionally, pathogen-mediated biofilm formation and β-lactamase production confer antibiotic resistance in approximately 37.6% of isolates, prolonging milk withdrawal periods and increasing the risk of drug residues, thereby posing threats to dairy safety (Shahzad et al., 2024; Chowdhury et al., 2025). Collectively, buffalo mastitis substantially diminishes milk yield and quality (Patil et al., 2015; Santos et al., 2020; Zhang et al., 2024), imposes serious economic losses (Das et al., 2018; Ali et al., 2021), and presents potential food safety hazards (X. Zhang et al., 2023; Singha et al., 2024).

Among the various pathogenic factors involved in mastitis, lipopolysaccharide (LPS), a major component of Gram-negative bacterial cell walls, serves as a key inducer of clinical mastitis in buffalo (Farmanullah et al., 2021). Buffalo mastitis manifests in either clinical or subclinical forms. The clinical form is characterized by mammary swelling, altered milk composition, elevated SCC, and may lead to irreversible damage or loss of mammary epithelial cells (MECs) (Baloch et al., 2024). In contrast, subclinical mastitis lacks visible symptoms but is characterized by a persistent elevation in SCC and reduced milk production, often serving as a silent reservoir for pathogen transmission. LPS engages toll-like receptor 4 (*TLR4*) on MECs, activating the nuclear factor-κB (*NF-κB*) and mitogen-activated protein kinase (MAPK) pathways. This activation drives the overexpression of pro-inflammatory cytokines, including interleukin-1 beta (*IL-1β*), interleukin-6 (*IL-6*), and tumor necrosis factor-α (*TNF-α*) (Salim et al., 2016; Védrine et al., 2024; S. Yan et al.,

2024). LPS also elevates reactive oxygen species (ROS) levels and myeloperoxidase (MPO) activity, triggering lipid peroxidation and DNA damage. Additionally, it activates JNK/MAPK pathways to upregulate pro-apoptotic proteins such as caspase-3 (*CASP3*) and Bcl-2-associated X protein(*Bax*), while downregulating the anti-apoptotic factor B-cell lymphoma 2 (*Bcl-2*), ultimately leading to MEC apoptosis (Geng et al., 2021). Furthermore, LPS suppresses the expression of genes essential for β-casein, lactose, and triglyceride synthesis, impairing mammary epithelial secretory function and reducing milk yield and quality (Liu et al., 2015; Tsugami et al., 2021). Single-cell transcriptomic analyses further demonstrate that LPS alters chromatin accessibility in peripheral blood monocytes, promoting inflammatory differentiation and downregulating lactation-related genes such as *SOSTDC1* and *WNT7B*, thereby exacerbating immune dysregulation and lactation dysfunction (Gao et al., 2022).

These LPS-induced pathological changes are intimately linked to metabolic reprogramming, as metabolic imbalance serves as a central driver of inflammation in MECs. Upon LPS stimulation, pro-inflammatory cytokines such as *TNF-α* and *IL-6* are secreted, which enhance glycolysis through both autocrine and paracrine mechanisms (Vaughan et al., 2013). *TNF-α* activates *NF-κB* and activator protein-1 (*AP-1*), leading to upregulation of pyruvate kinase M2 (*PKM2*) and increased lactate production, while *IL-6* promotes hexokinase 2 (*HK2*) activity via signal transducer and activator of transcription 3 (*STAT3*), thereby elevating glycolytic flux (Cheng et al., 2025; Y. Liu et al., 2025). *Staphylococcus* aureus triggers the ROS-HIF1α axis to upregulate *PFKFB3*, thereby driving cytokine production and amplifying inflammation (Gao et al., 2024). Similarly, Streptococcus uberis induces *HIF1α* through mTOR-dependent ROS signaling, increasing glycolysis and tissue damage; this effect can be alleviated by taurine through inhibition of HIF1α activity(Lan et al., 2022). Targeted metabolic interventions further highlight the therapeutic potential of modulating glycolysis: *PFKFB*3 inhibition attenuates both glycolysis and inflammatory responses, while S-allylmercaptocysteine (*SAMC*) suppresses LPS-induced *NF-κB* activation by regulating the TLR4/MyD88 pathway (Takashima et al., 2024). Additionally, leucine enhances β-casein synthesis and fatty acid metabolism via mTOR-PPARα signaling, underscoring the critical role of nutrition in maintaining metabolic immune homeostasis within the mammary gland (Huang et al., 2023).

This metabolic reprogramming triggers post-translational modifications,

particularly histone lactylation, which have recently emerged as critical regulators of inflammation. Lactate generated during glycolysis can be transported into the nucleus via monocarboxylate transporters, where it modifies histone lysine residues through p300/CBP, thereby linking cellular metabolism to epigenetic regulation (Xie et al., 2022; Hu et al., 2024; Ma et al., 2025). In MECs, LPS stimulation elevates MCT1 expression and enhances glycolytic flux, leading to lactate accumulation and subsequent induction of histone H3K18la (Jiang et al., 2022; Che et al., 2023). In sepsis-associated acute kidney injury, H3K18la enrichment at the RhoA promoter activates the RhoA/ROCK/Ezrin pathway, which triggers *NF-κB* activation, pro-inflammatory cytokine release, apoptosis, and renal dysfunction (Qiao et al., 2024). This pathological process is driven by glycolysis-derived lactate accumulation and can be attenuated by inhibiting lactate production or glucose uptake. In macrophages, histone lactylation regulates M1/M2 polarization through *p53* and *p300*, promoting VEGF-mediated tissue repair while suppressing excessive inflammation (Bao et al., 2025). Similarly, in glioma and endometrial carcinoma, lactylation enhances glycolysis by activating PI3K/AKT/HIF-1α signaling or stabilizing *PGK1*, thereby facilitating tumor progression and inhibiting apoptosis (Wei et al., 2024). Overall, histone lactylation integrates metabolic and epigenetic signaling to shape cellular fate in inflammatory contexts, highlighting its potential as a therapeutic target for inflammation-associated diseases. Despite these advances, the specific role of histone lactylation in buffalo mastitis remains largely unexplored.

Therefore, considering the critical role of histone lactylation in inflammatory regulation and the substantial economic impact of buffalo mastitis, this study aims to investigate the mechanisms underlying histone lactylation modifications and inflammatory injury in BuMECs. By elucidating these molecular pathways, we aim to establish a theoretical foundation for developing targeted therapeutic strategies for the prevention and treatment of mastitis in buffaloes.

MATERIALS AND METHODS

Animals

All animal experimental procedures were reviewed and approved by the Animal Ethics Committee of Guangxi University (Nanning, China; Approval No. GXU-2024-017). Lactating Murrah buffaloes were selected from the Buffalo Breeding Farm of the Guangxi Zhuang Autonomous Region Buffalo Research Institute. From a cohort of 118 buffaloes under identical rearing conditions, twelve

adult buffaloes in mid-lactation (aged 3-5 years, parity 1-3) were included. These were divided into two groups, six healthy controls with somatic cell counts (SCC) < 200,000 /mL, and six clinical mastitis cases with SCC > 500,000 /mL (Table 1), accompanied by typical clinical signs such as redness, swelling, heat, and pain in the mammary gland. Midstream milk samples were collected manually, immediately aliquoted, and transported to the laboratory for analysis. Blood samples were obtained via jugular venipuncture using EDTA-containing anticoagulant tubes, centrifuged at 2,000 r/min for 10 min at 4℃ to separate plasma, and stored at -80℃. Under local anesthesia and aseptic conditions, mammary tissue from the right rear quarter was collected. A portion of the tissue from healthy buffaloes was promptly processed for primary mammary epithelial cell isolation, while the remainder was snap-frozen in liquid nitrogen for subsequent protein/RNA extraction and sequencing, or fixed in 4% paraformaldehyde for histopathological evaluation. To further investigate the role of LPS in mastitis, a mouse model was established. Healthy postpartum mice (7-14 days postpartum) were randomly assigned to control and model groups, with ten mice per group. After intraperitoneal anesthesia and stabilization, the fourth pair of mammary glands in the model group were disinfected, and the nipple tips were trimmed by approximately 0.5-1 mm with sterile ophthalmic scissors to expose the lactiferous ducts. A volume of 50 μL of 0.2 mg/mL LPS solution was slowly infused via the ducts using a microsyringe. Control mice received an equal volume of sterile saline. After 24 hours of LPS induction, mice were euthanized by cervical dislocation. Blood was collected via cardiac puncture, centrifuged at 2,000 r/min for 10 min at 4℃ to obtain serum, and stored at -80℃. The fourth pair of mammary glands were aseptically harvested. one portion was fixed in 4% paraformaldehyde for histopathological assessment, and the other was flash-frozen in liquid nitrogen and transferred to -80℃ for subsequent protein and RNA analysis.

Cell culture and lipopolysaccharide treatment

BuMECs were cultured in DMEM/F12 medium (Gibco, C11330500BT, USA) supplemented with 10% fetal bovine serum (Gibco, A5256701, USA), 1 μg/mL hydrocortisone (Coolaber, CH6211-5g, China), 1 μg/mL progesterone (Sigma-Aldrich, V900699, USA), 5 μg/mL insulin (Sigma-Aldrich, I5500, USA), 5 μg/mL transferrin (McLin Biotech, T861419, China), and 10 ng/mL epidermal growth factor (Sigma-Aldrich, SRP3196, USA). Cells were seeded at 1×10^6 cells per dish and

maintained at 37°C in a humidified 5% CO_2 atmosphere. For LPS treatment (Sigma-Aldrich, L2630, USA), cells were exposed to increasing LPS concentrations (0, 1.25, 2.5, 5, or 10 μg/mL) for 12 h. In RNA interference assays, 10 μg/mL LPS was added 36 h post-transfection, followed by 12 h incubation before sample collection to assess LPS-induced effects on cellular responses and gene expression.

Immunohistochemistry staining

Mammary tissue samples were processed through deparaffinization, rehydration, and antigen retrieval using citrate buffer (Solarbio, C1033, China), with endogenous peroxidase quenched and non-specific binding blocked using goat serum. Sections were incubated with primary antibody (Supplementary Table S1) overnight at 4°C, followed by application of a biotinylated secondary antibody. Signals were detected using DAB (Solarbio, DA1015, China) or fluorescent substrates, accompanied by hematoxylin counterstaining, and final analysis was performed using a Nikon ECLIPSE Ts2-FL microscope (Nikon, Tokyo, Japan) to assess protein expression levels and localization.

Hematoxylin and eosin (H&E) staining

Mammary tissue samples were processed through deparaffinization, rehydration in graded ethanol, and staining with Mayer's hematoxylin (SenBeiJia, BP-DL001, China) for nuclear visualization, followed by differentiation in 0.5% acid alcohol (Solarbio, G1861, China) and counterstaining with alcoholic eosin (SenBeiJia, BP-DL001, China) to enhance cellular contrast. After dehydration through ethanol series and clearing in xylene, sections were mounted with neutral resin (Solarbio, G8590, China) and examined using a Nikon ECLIPSE Ts2-FL microscope (Nikon, Tokyo, Japan) for morphological and histological assessment.

TUNEL staining

The TUNEL assay was performed to detect apoptotic cells in paraffin-embedded mammary tissue sections. The process began with deparaffinization using xylene, followed by rehydration through a graded ethanol series. Sections were then treated with proteinase K (Servicebio, G1205, China) for 30 minutes at 37°C to expose DNA fragments. After PBS washes, endogenous peroxidase activity was quenched with 3% H_2O_2. The TUNEL reaction mixture, containing terminal deoxynucleotidyl transferase (TdT) and labeled dUTP (Servicebio, G1507, China), was applied to the sections and incubated at 37°C for 1 hour. Signals were developed using DAB substrate (Servicebio, G1221, China), and sections were counterstained with hematoxylin.

Immunofluorescence staining

BuMECs were fixed with paraformaldehyde (Solarbio, P1110, China), permeabilized with Triton X-100 (Solarbio, T8200, China), and blocked with bovine serum albumin (Sigma-Aldrich, A9418, USA). Primary antibodies (Supplementary Table S1) were applied overnight at 4°C, followed by incubation with fluorochrome-conjugated secondary antibodies (Supplementary Table S1) and nuclear counterstaining using Hoechst 33342 (Solarbio, B8040, China). Images were acquired with a Nikon ECLIPSE Ts2-FL microscope (Nikon, Tokyo, Japan).

Detection of lipopolysaccharides

LPS concentrations in buffalo mammary tissue, milk, and serum were quantified using a Limulus Amebocyte Lysate (LAL) assay kit (Solarbio, T7575, China). Sample processing followed manufacturer's instructions, serum was obtained from anticoagulated blood via centrifugation, diluted 1:9 in processing solution, and heat-treated at 70°C for 10 min. Milk samples were centrifuged to remove fat, with the middle phase collected, diluted 1:19, and similarly heat-treated. Tissue samples (30 mg) were homogenized, diluted 1:9, and subjected to identical heat treatment. Data collection involved measuring optical density at 545 nm using a microplate reader (BioTek, Epoch2TC, USA), and analysis comprised generating a standard curve from serial dilutions of a 20 EU/mL LPS stock to calculate LPS concentrations.

Myeloperoxidase (MPO) activity detection

MPO activity in mammary tissue was assayed using a myeloperoxidase kit (Nanjing Jiancheng, A044-1-1, China) per manufacturer's protocol. The samples were homogenized on ice to create a 5% homogenate, followed by an assay procedure involving incubation with specific reagents at 37°C, chromogenic reaction, and termination. Data collection involved measuring optical density at 460 nm with a microplate reader (BioTek, Epoch2TC, USA), and analysis comprised calculating MPO activity from a standard curve.

Western blot analysis

Mammary tissue or BuMECs samples were selected and homogenized in lysis buffer, with protein concentrations determined using a BCA assay kit (Biosharp, BL521A, China) to ensure consistent loading. Equal protein amounts (20 μg) were mixed with SDS loading buffer, denatured at 100°C for 10 min, and separated by SDS-PAGE. Proteins were then transferred to nitrocellulose membranes (Solarbio, YA1711, China) via wet transfer at 300 mA for 1.5 h. For data collection, membranes were blocked

with 5% nonfat milk in PBST, incubated overnight at 4°C with primary antibodies (Supplementary Table S1), washed, and probed with HRP-conjugated secondary antibodies, followed by visualization using an ECL kit (Tanon, 180-506, China) and imaging with an E-Blot Touch Imager (VonLab, Shanghai, China). Analysis involved quantifying band intensities with ImageJ software (NIH, v1.54, USA), using β-actin or histone H3 as loading controls for normalization.

Quantitative real-time quantitative PCR (qPCR) analysis

Total RNA was isolated from biological samples using an RNA extraction kit (TaKaRa, 9767, Japan) and reverse transcribed into cDNA using the manufacturer's protocol. The cDNA was appropriately diluted, and qPCR reactions were prepared in a 10 μL volume containing gene-specific primers (Tables S2 and S3), PerfectStart Green qPCR SuperMix (TransGen, AT341, China), and nuclease-free water. Data collection involved amplification on a LightCycler 480 system (Roche, Mannheim, Germany) under standardized conditions: initial denaturation at 95°C for 5 min, followed by 40 cycles of 95°C for 10 s and 60°C for 30 s. Analysis utilized the $2^{-\Delta\Delta CT}$ method with β-actin as the internal reference gene for calculating relative transcript abundance, ensuring transparency and reproducibility, while primers were designed based on GenBank sequences (NCBI) and synthesized by Shanghai Bioengineering Co., Ltd. (Shanghai, China).

ELISA detection

BuMECs culture supernatants were selected as samples and processed by centrifugation to remove cellular debris. Standards and appropriately diluted samples were added to 96-well plates provided in the assay kits (Jiangsu Enzyme, MM-3473602 and MM-156802, China) and incubated at 37°C to facilitate antigen-antibody binding. After washing steps, wells were incubated with enzyme-conjugated detection antibody, followed by substrate addition for color development. Data collection involved measuring optical density at 450 nm using a microplate reader (BioTek, Epoch2TC, USA), and analysis comprised calculating analyte concentrations from standard curves to enable quantitative determination of target proteins, ensuring methodological transparency and reproducibility throughout the process.

Flow cytometry analysis

BuMECs were selected as samples and processed through harvesting, washing with PBS, and preparation of a single-cell suspension using trypsinization and

centrifugation with a benchtop centrifuge (CENCE, TD5A-WS, China). The cells were resuspended in binding buffer and stained with Annexin V–FITC and propidium iodide (BD Biosciences, 559763, USA) for 30 minutes at room temperature in the dark to facilitate apoptosis detection. Data collection was conducted by immediately analyzing the stained cells using a flow cytometer (Beckman Coulter, CytoFlew S, USA), and analysis involved processing the acquired data with FlowJo software (Tree Star, v10.0.7, USA) to quantify apoptotic populations, emphasizing methodological transparency and operational reproducibility throughout the process.

Lactate level analysis

Lactate concentrations in buffalo mammary tissue and BuMECs were determined using a lactate detection kit (Abbkine, KTB1100, China) according to the manufacturer's instructions. Briefly, samples were processed following the kit protocol, and absorbance was measured at 450 nm using an automatic microplate reader (BioTek, Epoch2TC, USA). Lactate concentrations were calculated from standard curves generated in parallel, allowing quantitative assessment of lactate levels in each sample.

RNA-seq analysis

BuMECs were selected as biological samples, and total RNA was extracted using TRIzol reagent (Servicebio, G3013-100ML, China) per manufacturer's protocol, with RNA quality assessed via Agilent 2100 Bioanalyzer (Agilent, USA) and NanoDrop spectrophotometer (Thermo Fisher, USA) to ensure integrity. RNA-seq libraries were constructed with the NEBNext Ultra RNA Library Prep Kit (NEB, USA) including three biological replicates per group, and sequenced on a BGISeq platform (BGI, China) to generate 150 bp paired-end reads. Data collection involved converting raw reads to FASTQ format, performing quality control with FastQC, and trimming adapters/low-quality bases using Trimmomatic. Clean reads were aligned to the buffalo reference genome (NCBI assembly) with STAR, and BAM files were processed with SAMtools for sorting and indexing. Analysis included differential expression evaluation using DESeq2 in R with thresholds of $|\log_2 FC| \geq 1$ and adjusted $P<0.05$, followed by functional enrichment analysis for KEGG pathways with DAVID Bioinformatics Resources to ensure methodological transparency and reproducibility.

CUT&Tag analysis

BuMECs were selected as biological samples and processed using the Hyperactive Universal CUT&Tag Assay Kit (Vazyme, TD903, China) per manufacturer's protocol

to ensure operational transparency. The experimental design involved binding cells to protein A-coated magnetic beads and sequential incubation with ConA beads, anti-H3K18la primary antibody, secondary antibody, and hyperactive pA/G-Tn5 transposase for targeted chromatin fragmentation. DNA fragments were extracted, PCR-amplified, purified, and used to construct sequencing libraries, which were quantified and quality-checked with a Qubit 4.0 fluorometer (Thermo Fisher, USA) and an Agilent 2100 Bioanalyzer (Agilent, USA). Data collection comprised sequencing indexed libraries on an Illumina NovaSeq 6000 platform (Illumina, USA) to generate 150 bp paired-end reads, followed by quality assessment with FastQC and adapter trimming with Trimmomatic to obtain clean reads. Analysis steps included aligning clean reads to the buffalo reference genome (NCBI assembly) using Bowtie2, sorting and indexing BAM files with SAMtools, generating BedGraph files with Bedtools, calling peaks with SEACR under low-background conditions, conducting differential peak analysis with DESeq2 in R, and visualizing chromatin landscapes with Integrative Genomics Viewer.

Statistical analysis

All quantitative data are presented as mean±SD from at least three independent biological replicates. Pairwise comparisons were performed using unpaired two-tailed Student's t-test. For comparisons involving three or more groups, one-way analysis of variance (ANOVA) with Tukey's post hoc test was used. Different lowercase letters above bars indicate significant differences among groups (P<0.05). Asterisks denote statistical significance: *: P<0.05; **: P<0.01, ***: P<0.001. A threshold of P<0.05 was considered statistically significant. All statistical analyses and graphical outputs were generated using GraphPad Prism 8.0.1.

RESULTS

LPS induces exacerbated inflammatory injury in buffalo mammary tissue

Histological exam ination revealed extensive neutrophil infiltration in both interstitial and alveolar regions of CM mammary tissues (Figure 1A), accompanied by markedly increased MPO activity compared with controls (Figure 1B). qPCR analysis demonstrated significant upregulation of *IL-1β*, *IL-6*, *TNF-α*, *TLR4*, and *NF-κB* in CM tissues (Figure 1C), which was corroborated by elevated TLR4, NF-κBp65, and IL-6 protein expression detected by Western blot (Figure 1D). Apoptotic activity was elevated in CM, as shown by TUNEL staining (Figure 1E), together with increased expression of pro-apoptotic *BAX* and *CASP3* and reduced expression of anti-apoptotic

Bcl-2 at both the mRNA (Figure 1F) and protein levels (Figure 1G). LAL assay confirmed that LPS, a major pathogenic factor in mastitis, was significantly increased in milk, mammary tissue, and serum of buffaloes with CM (Figure 1H). Immunohistochemistry further demonstrated enhanced LPS distribution and intensity within mammary tissues (Figure 1I). These findings were further validated in an LPS-induced mouse mastitis model, which exhibited marked increases in inflammatory and apoptotic markers 24 h post-injection (Figure 1J-L; Supplementary Figure S1A-E).

LPS Induces inflammation and apoptosis in BuMECs in vitro

BuMECs were successfully isolated and confirmed by keratin 18 immunofluorescence, displaying typical morphology and stable function at passage 3 (Supplementary Figure S2A-E). An in vitro inflammatory injury model was established by treating BuMECs with different concentrations of LPS for 12 h. Cell viability declined in a dose-dependent manner with increasing LPS concentrations (Figure 2A). ELISA showed that IL-6 and TNF-α secretion peaked at 10 μg/mL LPS (Figure 2B). qPCR analysis revealed concentration-dependent upregulation of *IL-1β*, *IL-6*, *TNF-α*, *TLR4*, and *NF-κB*, with maximal induction at 10 μg/mL (Figure 2C). Further qPCR confirmed that *IL-6*, *TNF-α*, *TLR4*, and *NF-κB* expression increased progressively with higher LPS doses (Figure 2D-G). Accordingly, 10 μg/mL LPS was selected for subsequent experiments. Flow cytometry demonstrated that LPS substantially increased apoptosis (Figure 2H) and enhanced CASP3 fluorescence intensity (Figure 2I). These findings were supported by qPCR showing elevated expression of pro-apoptotic *BAX* and *CASP3* and reduced *Bcl-2* (Figure 2J), with consistent results at the protein level confirmed by Western blot (Figure 2K).

LPS upregulates glycolytic activity in BuMECs

RNA-seq identified 5,382 differentially expressed genes between control and LPS-treated groups, including 2,995 upregulated and 2,387 downregulated genes (Figure 3A). KEGG pathway enrichment analysis revealed that LPS treatment significantly activated pathways related to inflammation, apoptosis, and metabolic processes including glycolysis and gluconeogenesis (Figure 3B). Furthermore, GSEA demonstrated a marked upregulation of the glycolysis/gluconeogenesis pathway in the LPS treatment (Figure 3C), and heatmap analysis indicated enhanced expression of glycolytic genes (Figure 3D), collectively suggesting that LPS stimulation strongly promotes activation of glycolytic metabolic pathways. qPCR and Western blot

analyses confirmed significant upregulation of glycolytic enzymes *HK2*, *PKM2*, *PDK2*, and *LDHA* following LPS treatment (Figure 3E, F). Protein-protein interaction (PPI) network analysis further identified *HK2* as a central node within the glycolytic network, highlighting its potential as a key regulator of glycolytic flux (Figure 3G).

Inflammation leads to lactate accumulation and increased histone lactylation levels in BuMECs

LPS treatment consistently increased both intracellular and extracellular lactate levels in BuMECs (Figure 4A), paralleling the elevated lactate concentrations detected in milk, mammary tissue, and serum from buffaloes with clinical mastitis compared with healthy controls (Supplementary Figure S3A). Western blot analysis further demonstrated a robust upregulation of Pankla following LPS stimulation (Figure 4B). Among multiple histone lactylation sites examined, H3K18la exhibited the most pronounced increase in response to LPS treatment (Figure 4C). These findings were corroborated by immunofluorescence, which confirmed elevated PanKla and H3K18la in LPS-treated BuMECs (Figure 4D, E), and by immunohistochemistry, which revealed higher expression of these markers in mammary tissues from mastitis-affected buffaloes (Supplementary Figure S3B).

H3K18 lactylation modifications promotes inflammation and apoptosis in BuMECs

Quality control of CUT&Tag sequencing demonstrated significantly higher signal enrichment near gene regions in LPS-treated BuMECs compared with controls (Figure 5A). Peak analysis identified 5,813 regions with increased signals and 3,904 with decreased signals following LPS exposure (Supplementary Figure S3C, D). Integrated analysis with RNA-seq data through a nine-quadrant correlation plot revealed 170 candidate genes consistently upregulated in both datasets, demonstrating concurrent elevation of H3K18la enrichment at promoters and corresponding increases in mRNA transcript levels (Figure 5B, C). Among these, *NF-κB1*, *CEBPD*, and *DDIT3* were identified as key regulators associated with inflammatory and apoptotic pathways (Figure 5D). IGV visualization further confirmed significant enrichment of H3K18la peaks at the promoters of these genes, including *DDIT3* peaks 43,616 and 43,617, *NF-κB1* peak 73,523, and *CEBPD* peak 126,773, all of which were considerably upregulated in LPS-treated samples relative to controls (Figure 5E-G).

Inhibition of HK2 reduces H3K18 lactylation levels and alleviates inflammatory

injury in BuMECs

HK2 occupies a central position in the glycolytic network, serving as the rate-limiting enzyme that governs glycolytic flux and subsequent lactate production. To determine whether H3K18la accumulation and the downstream inflammatory/apoptotic responses are strictly dependent on this upstream metabolic driver, we targeted *HK2* for knockdown to disrupt the lactate supply chain. RNA interference targeting *HK2* in LPS-treated BuMECs effectively reduced *HK2* expression along with *PKM2*, *PDK2*, and *LDHA* (Figure 6A; Supplementary Figure S3E). *HK2* knockdown significantly decreased lactate production despite LPS stimulation (Figure 6B) and markedly lowered H3K18la levels (Figure 6C). Western blot showed that silencing HK2 reduced TLR4, NF-κBp65, and IL-6 protein expression and decreased pro-apoptotic BAX and CASP3 while restoring anti-apoptotic Bcl-2 (Figure 6D, E). qPCR further confirmed significant downregulation of *IL-1β*, *IL-6*, *TNF-α*, and *TLR4* (Figure 6F), as well as *BAX* and *CASP3*, with concomitant upregulation of *Bcl-2* (Figure 6G). Moreover, expression of *NF-κB1*, *CEBPD*, and *DDIT3* was markedly decreased following *HK2* knockdown (Figure 6H).

DISCUSSION

Mastitis in water buffalo is a major factor contributing to reduced milk production and poses potential risks to food safety. Lipopolysaccharide, a principal component of Gram-negative bacterial cell walls, is a primary etiological factor in clinical mastitis (Meng et al., 2022; Xie et al., 2024). Previous studies in bovines have indicated that clinical mastitis is associated with altered mammary metabolism and increased lactate accumulation, suggesting that lactate may influence epigenetic modifications, including histone lactylation (Ma et al., 2025). Despite growing evidence of metabolic-epigenetic crosstalk in inflammation, the precise mechanisms linking LPS-induced lactate accumulation to histone lactylation remain poorly characterized. This study aimed to elucidate the mechanistic links between LPS-induced lactate accumulation, histone lactylation dynamics, and their regulatory effects on inflammatory and apoptotic pathways in BuMECs.

Our results revealed that LPS exposure triggers profound metabolic reprogramming in BuMECs, characterized by significant upregulation of key glycolytic enzymes including *HK2*, *PKM2*, *PDK2*, and *LDHA*. This glycolytic shift is consistent with the "Warburg-like" metabolic reprogramming observed in activated immune cells and inflamed tissues (Wu et al., 2020; Song et al., 2023). Although similar glycolytic

activation has been documented in bovine mastitis models (Ma et al., 2025; Cheng et al., 2025), the specific role of *HK2* as a master regulator controlling this process remained unclear. Our PPI network analysis uniquely identified *HK2* as the central hub gene with the highest connectivity, positioning it as the rate-limiting checkpoint controlling downstream lactate production (Bao et al., 2022). This is critical because *HK2* catalyzes the first irreversible step of glycolysis, making it the most upstream and efficient target for therapeutic intervention.

Importantly, our findings demonstrate that this enhanced glycolytic flux directly drives lactate accumulation in BuMECs, with intracellular lactate levels increasing significantly following LPS stimulation. This lactate surge was accompanied by marked upregulation of multiple histone lactylation modifications, including PanKla, H3K9la, H3K56la, H3K18la, H4K5la, and H4K8la. Notably, H3K18la exhibited the most pronounced elevation. This site-specific selectivity is biologically significant, as H3K18la has been established as a canonical active transcriptional mark associated with promoter regions and gene activation, making it the most functionally relevant target for investigating inflammatory gene regulation (Zhang et al., 2019). H3K18la enrichment at specific promoters provides a direct mechanistic link between metabolic dysregulation and transcriptional activation of inflammatory effectors.

CUT&Tag analysis revealed the critical role of H3K18la in transcriptional regulation, demonstrating its enrichment at the promoter regions of key inflammatory and apoptotic genes, including *DDIT3*, *NF-κB1*, and *CEBPD*. Lactate stimulation significantly increased H3K18la levels in the promoter regions of these genes, promoting their transcriptional activation (Wang et al., 2024; S. Liu et al., 2025). *NF-κB1*, a core transcription factor involved in the inflammatory response, exhibited an approximately 4-fold increase in expression, consistent with previous findings on the role of H3K18la in regulating inflammatory responses (Wei et al., 2023; Wan et al., 2025). Importantly, *NF-κB1* upregulation creates a positive feedback loop, as NF-κB signaling further enhances glycolysis through transcriptional activation of *HK2* and *LDHA*, thereby amplifying lactate production and H3K18la modification (Cheng et al., 2025). *CEBPD*, an important transcription factor with H3K18la-modified promoter regions, participates in cellular inflammatory cascade reactions and promotes apoptosis (Yu et al., 2010; T. Yan et al., 2024). *DDIT3*, involved in inflammatory mRNA processing and immune response regulation, showed increased H3K18la promoter modification, consistent with recent reports on

lactate-mediated inflammatory gene regulatory mechanisms in cells (Kim et al., 2017; Y. Zhang et al., 2023).

These findings implicate the HK2-lactate-H3K18la axis as a central regulatory pathway (Figure 7). Therefore, to validate the functional significance of the HK2-lactate-H3K18la axis, we employed *HK2* inhibition as a targeted intervention strategy. Given that lactate serves as a critical modifier for H3K18la activation and *HK2* functions as a key regulator of lactate metabolism, we investigated the role of H3K18la in BuMECs by inhibiting *HK2* activity. Using siRNA-mediated interference, we effectively downregulated *HK2* expression, resulting in significant reductions in *HK2*, *PKM2*, *PDK2*, and *LDHA* levels and substantial attenuation of glycolytic activity. Subsequent lactate measurements demonstrated a significant decrease in intracellular lactate levels following *HK2* knockdown, accompanied by corresponding reductions in H3K18la modification. Furthermore, *HK2* knockdown led to marked reductions in inflammatory cytokine expression and apoptotic indices, indicating that HK2-mediated glycolysis critically contributes to LPS-induced inflammatory injury in BuMECs. These results collectively suggest that targeting *HK2* and the lactate-H3K18la axis may provide a promising approach for modulating inflammatory responses in mastitis.

While the glycolysis-lactate-histone lactylation axis has been recently explored in bovine mammary epithelial cells (Ma et al., 2025; Cheng et al., 2025), our study provides novel insights specific to the water buffalo, a species known for its distinct disease resistance traits compared to Bos taurus. Unlike previous studies that largely focused on broad lactylation (Pankla) changes or canonical HIF-1α signaling using candidate gene approaches, we utilized high-resolution CUT&Tag profiling to specifically identify H3K18la as a key epigenetic driver. Crucially, this epigenomic mapping revealed *DDIT3* and *CEBPD* as novel direct targets of H3K18la in buffalo cells targets not previously reported in the bovine mastitis context. This suggests that while the broad metabolic-epigenetic strategy is conserved across ruminants, the specific chromatin targets and regulatory networks may have diverged, potentially contributing to the unique inflammatory response patterns observed in buffalo.

Collectively, our faceted investigation reveals a novel mechanistic pathway in which LPS-driven metabolic reprogramming triggers H3K18la-mediated epigenetic regulation, establishing H3K18la as a critical molecular bridge that links cellular metabolism to inflammatory and apoptotic responses in mastitis. Targeting the

HK2-lactate-H3K18la axis represents a promising therapeutic strategy for modulating inflammation in buffalo mammary tissues. Despite these advances, certain limitations should be acknowledged. Direct functional validation through site-directed H3K18 mutagenesis and isotope tracing experiments to definitively establish lactate metabolic origin remain technically challenging in BuMECs. Future investigations should therefore prioritize in vivo validation using buffalo mastitis models, develop mammary-targeted delivery systems for *HK2* inhibitors or RNAi therapeutics, and explore pharmacological modulation of histone lactylation writers as complementary strategies to validate the clinical potential of this pathway.

CONCLUSION

In conclusion, our findings demonstrate that LPS-induced inflammation in BuMECs promotes glycolysis and increases lactate production, thereby enhancing histone lactylation, particularly H3K18la. H3K18la modification facilitates the recruitment of transcriptional regulators, including *DDIT3*, *NF-κB1*, and *CEBPD*, which activate key inflammation and apoptosis genes, thereby driving inflammatory injury. Inhibition of *HK2* reduces lactate accumulation and H3K18la levels, thus mitigating inflammation and apoptosis. These results provide novel insights into the epigenetic mechanisms regulating the pathogenesis of buffalo mastitis.

SUPPLEMENTARY DATA

Supplementary data to this article can be found online.

DATA AVAILABILITY

The raw sequencing data have been deposited in the Genome Sequence Archive (GSA) at the China National Center for Bioinformation (https://ngdc.cncb.ac.cn/gsa) under Project accession numbers PRJCA055308 (RNA-seq) and PRJCA055375 (CUT&Tag). All data that support the findings of this study are available from the corresponding authors upon request.

COMPETING INTERESTS

The authors declare that they have no competing interests.

AUTHORS' CONTRIBUTIONS

X.W.L. and J.H.S designed the experiments. P.X. performed the experiments and completed the manuscript. X.R.T., J.C.Z. and B.Z. performed the cell experiments. M.Q.L. preformed animal experiments. C.Y.Y., M.J.C and H.Y.Z. analyzed CUT&Tag and RNA-Seq data. P.X. and X.G.Y. analyzed most of the experimental data. All

authors read and approved the final version of the manuscript.

FOUNDATION ITEMS

This work was supported by the National Key R&D Program of China (No.2022YFD160010X), the National Natural Science Foundation of China (No. 82160287, No. 32372881), the Guangxi Science and Technology Major Project (GuiKe AA24263009), the Central Government Guided Local Science and Technology Development Fund (GuangXi)(GuiKe ZY24212019), the earmarked fund for CARSGIT (nycytxgxcxtd-2021-21-01), and the Guangxi Vocational University of Agriculture Scientific Research and Technological Development Project (XKJ2326).

REFERENCES

Ali T, Kamran, Raziq A, et al. 2021. Prevalence of mastitis pathogens and antimicrobial susceptibility of isolates from cattle and buffaloes in northwest of pakistan. *Frontiers in Veterinary Science*, **8**: 746755.

Baloch H, Rind R, Kalhoro DH, et al. 2024. Influence of bacterial species on physical characteristics and somatic cell counts in clinical and subclinical mastitis milk of kundhi buffaloes. *Pakistan Journal of Zoology*, **3**(56):1-9.

Bao CC, Ma Q, Ying XH, et al. 2025. Histone lactylation in macrophage biology and disease: from plasticity regulation to therapeutic implications. *EBioMedicine*, **111:** 105502.

Bao CC, Zhu SY, Song KP, et al. 2022. *HK2*: a potential regulator of osteoarthritis via glycolytic and non-glycolytic pathways. *Cell Communication and Signaling*, **20**(1)**:** 132.

Che HY, Zhou CH, Liu CC, et al. 2023. Allicin alleviated LPS-induced mastitis via the TLR4/NF-κB signaling pathway in bovine mammary epithelial cells. *International Journal of Molecular Sciences*, **24**(4): 3805.

Cheng XY, Jiang YJ, Zhao X, et al. 2025. Regulation of lactate accumulation in bovine mammary epithelial cells by LPS-induced HIF-1α/MCT1 pathway. *Microbial Pathogenesis*, **199**: 107261.

Chowdhury MS, Hossain H, Rahman MN, et al. 2025. Emergence of highly virulent multidrug and extensively drug resistant escherichia coli and klebsiella pneumoniae in buffalo subclinical mastitis cases. *Scientific Reports*, **15**(1): 11704.

Costa A, Neglia G, Campanile G, et al. 2020. Milk somatic cell count and its relationship with milk yield and quality traits in italian water buffaloes. *Journal of Dairy Science*, **103**(6), 5485–5494.

Das D, Panda SK, Jena B, et al. 2018. Economic impact of subclinical and clinical mastitis in odisha, india. *International Journal of Current Microbiology and Applied Sciences*, **7**(3): 3651-3654.

Farmanullah F, Gouda M, Zhang M, et al. 2021. The variation in promoter sequences of the AKT3 gene between cow and buffalo revealed different responses against mastitis. *Journal of Genetic Engineering and Biotechnology*, **19**(1): 164.

Gao X, Wang ZL, Xu YY, et al. 2024. PFKFB3-meditated glycolysis via the reactive oxygen species–hypoxic inducible factor 1α axis contributes to inflammation and proliferation of *staphylococcus aureus*in epithelial cells. *The Journal of Infectious Diseases*, **229**(2): 535-546.

Gao YH, Li JB, Cai GZ, et al. 2022. Single-cell transcriptomic and chromatin accessibility analyses of dairy cattle peripheral blood mononuclear cells and their responses to lipopolysaccharide. *Bmc Genomics*, **23**(1): 338.

Geng ZJ, Shan XF, Lian S, et al. 2021. LPS-induced SOCS3 antagonizes the JAK2-STAT5 pathway and inhibits β-casein synthesis in bovine mammary epithelial cells. *Life Sciences*, **278**: 119547.

Hu Y, He ZL, Li ZJ, et al. 2024. Lactylation: the novel histone modification influence on gene expression, protein function, and disease. *Clinical Epigenetics*, **16**(1)**:** 72.

Huang JT, Li JT, Ning Y, et al. 2023. Enhancement of PPARα-inhibited leucine metabolism-stimulated β-casein synthesis and fatty acid synthesis in primary bovine mammary epithelial cells. *Journal of Agricultural and Food Chemistry*, **71**(43): 16184-16193.

Jiang MC, Lv ZY, Huang YH, et al. 2022. Quercetin alleviates lipopolysaccharide-induced inflammatory response in bovine mammary epithelial cells by suppressing TLR4/NF-κB signaling pathway. *Frontiers in Veterinary Science*, **9**: 915726.

Kim JY, Song HS, Heo HR, et al. 2017. Cadmium-induced ER stress and

inflammation are mediated through c/EBP–DDIT3 signaling in human bronchial epithelial cells. *Experimental & Molecular Medicine*, **49**(9): e372.

Lan RG, Zhou YY, Wang ZL, et al. 2022. Reduction of ROS-HIF1α-driven glycolysis by taurine alleviates*streptococcus uberis* infection. *Food & Function*, **13**(4): 1774-1784.

Liu LX, Lin Y, Liu LL, et al. 2015. 14-3-3γ regulates lipopolysaccharide-induced inflammatory responses and lactation in dairy cow mammary epithelial cells by inhibiting NF-κB and MAPKs and up-regulating mTOR signaling. *International Journal of Molecular Sciences*, **7**(16): 16622-16641.

Liu ST, He YT, Jin LL, et al. 2025. H3K18 lactylation-mediated SIX1 upregulation contributes to silica-induced epithelial-mesenchymal transition in airway epithelial cells. *Toxicology*, **514**: 154109.

Liu YF, Gong Z, Zhang LF, et al. 2025. Esketamine attenuates traumatic brain injury by modulating STAT3-mediated glycolysis and immune responses. *Bmc Neuroscience*, **26**(1): 21.

Ma N, Wang LR, Meng MJ, et al. 2025. D-sodium lactate promotes the activation of NF-κB signaling pathway induced by lipopolysaccharide via histone lactylation in bovine mammary epithelial cells. *Microbial Pathogenesis*, **199:** 107198.

Meng MJ, Huo R, Wang Y, et al. 2022. Lentinan inhibits oxidative stress and alleviates LPS-induced inflammation and apoptosis of BMECs by activating the Nrf2 signaling pathway. *International Journal of Biological Macromolecules*, **222**(Pt B), 2375–2391.

Patbandha TK, Marandi S, Ravikala K, et al. 2015. Association of milk components with intra-mammary inflammation in jaffrabadi buffaloes. *Veterinary World*, **8**(8)**:** 989-993.

Patil MP, Nagvekar AS, Ingole SD, et al. 2015. Somatic cell count and alkaline phosphatase activity in milk for evaluation of mastitis in buffalo. *Veterinary World*, **8**(3): 363-366.

Puggioni GM, Tedde V, Uzzau S, et al. 2020. Evaluation of a bovine cathelicidin ELISA for detecting mastitis in the dairy buffalo: comparison with milk somatic

cell count and bacteriological culture. *Research in Veterinary Science*, **128**: 129-134.

Qiao J, Tan Y, Liu HC, et al. 2024. Histone H3K18 and ezrin lactylation promote renal dysfunction in sepsis-associated acute kidney injury. *Advanced Science*, **11**(28): e2307216.

Salim TH, Sershen CL, May EE. 2016. Investigating the role of *TNF-α* and *IFN-γ* activation on the dynamics of *iNOS* gene expression in LPS stimulated macrophages. *PLoS One*, **11**(6): e0153289.

Santos AD, Lima DC, Abad AC, et al. 2020. Antimicrobial resistance profile of non-aureus*staphylococci* isolates from buffalo, goat and sheep mastitis in the northeast region of brazil. *Journal of Dairy Research*, **87**(3): 290-294.

Shahzad MA, Yousaf A, Ahsan A, et al. 2024. Virulence and resistance` profiling of staphylococcus aureus isolated from subclinical bovine mastitis in the pakistani pothohar region. *Scientific Reports*, **14**(1): 14569.

Singha S, Koop G, Rahman MM, et al. 2024. Pathogen group-specific risk factors for intramammary infection in water buffalo. *PLoS One*, **19**(4): e0299929.

Song H, Lu ZQ, Zhan K, et al. 2023. Effects of glucose levels on inflammation and amino acid utilization in lipopolysaccharide-induced bovine mammary epithelial cells. *Animals*, **13**(22): 3494.

Takashima M, Kurita M, Terai H, et al. 2024. S-allylmercaptocysteine inhibits TLR4-mediated inflammation through enhanced formation of inhibitory MyD88 splice variant in mammary epithelial cells. *Scientific Reports*, **14**(1): 29627.

Tsugami Y, Wakasa H, KM, et al. 2021. Lipopolysaccharide and lipoteichoic acid influence milk production ability via different early responses in bovine mammary epithelial cells. *Experimental Cell Research*, **400**(2): 112472.

Vaughan RA, Garcia SR, Dorsey J, et al. 2013. Tumor necrosis factor alpha induces warburg‐like metabolism and is reversed by anti-inflammatory curcumin in breast epithelial cells. *International Journal of Cancer*, **133**(10): 2504-2510.

Védrine M, Gilbert FB, Maman S, et al. 2024. Soluble CD14 produced by bovine mammary epithelial cells modulates their response to full length LPS. *Veterinary*

Research, **55**(1): 76.

Wan LL, Zhang HJ, Liu JL, et al. 2025. Lactylation and human disease. *Expert Reviews in Molecular Medicine*, **27**: e10.

Wang PW, Xie DX, Xiao T, et al. 2024. H3K18 lactylation promotes the progression of arsenite-related idiopathic pulmonary fibrosis via YTHDF1/m6a/NREP. *Journal of Hazardous Materials*, **461**: 132582.

Wei L, Yang XW, Wang J, et al. 2023. H3K18 lactylation of senescent microglia potentiates brain aging and alzheimer's disease through the NF-κB signaling pathway. *Journal of Neuroinflammation*, **20**(1): 208.

Wei ST, Zhang J, Zhao R, et al. 2024. Histone lactylation promotes malignant progression by facilitating *USP39* expression to target PI3k/AKT/HIF-1α signal pathway in endometrial carcinoma. *Cell Death Discovery*, **10**(1): 121.

Wu YJ, Sun YW, Dong XW, et al. 2020. The synergism of PGN, LTA and LPS in inducing transcriptome changes, inflammatory responses and a decrease in lactation as well as the associated epigenetic mechanisms in bovine mammary epithelial cells. *Toxins*, **12**(6): 387.

Xie YC, Li XY, Xu DW, et al. 2024. Hordenine alleviates lipopolysaccharide-induced mastitis by suppressing inflammation and oxidative stress, modulating intestinal microbiota, and preserving the blood milk barrier. *Journal of Agricultural and Food Chemistry*, **72**(39): 21503-21519.

Xie YM, Hu HX, Liu MT, et al. 2022. The role and mechanism of histone lactylation in health and diseases. *Frontiers in Genetics*, **13**: 949252.

Yan SP, Ju XH, Lao JL, et al. 2024. Overexpression of the *Mas1* gene mitigated LPS-induced inflammatory injury in mammary epithelial cells by inhibiting the NF-κb/MAPKs signaling pathways. *Frontiers in Veterinary Science*, **11**: 1446366.

Yan TT, Yan NN, Xia YL, et al. 2024. Hepatocyte-specific CCAAT/enhancer binding protein α restricts liver fibrosis progression. *Journal of Clinical Investigation*, **134**(7): e166731.

Yu XY, Si JL, Zhang YJ, et al. 2010. CCAAT/enhancer binding protein-delta (c/EBP-delta) regulates cell growth, migration and differentiation. *Cancer Cell*

International, **10**(1)**:** 48.

Zhang D, Tang Z, Huang H, et al. 2019. Metabolic regulation of gene expression by histone lactylation. *Nature*, **574**(7779): 575-580.

Zhang XX, Li Y, Zhang YP, et al. 2024. A new method to detect buffalo mastitis using udder ultrasonography based on deep learning network. *Animals*, **5**(14): 707.

Zhang XX, Niu KF, Wang W, et al. 2023. Relationships between body and udder related type traits with somatic cell counts and potential use for an early selection method for water buffaloes (*bubalus bubalis*). *Journal of Animal Science*, **101**: skad238.

Zhang YW, Duan ZW, Guan YH, et al. 2023. Identification of 3 key genes as novel diagnostic and therapeutic targets for OA and COVID-19. *Frontiers in Immunology*, **14**: 1167639.

Table 1. Basic description of buffaloes classified as healthy (Control, n=6) or clinical mastitis (CM, n=6)

Item	Median (IQR)	
	Control	CM
SSC (10^4cells/mL)	4.72(0.075)b	65.85(9.972)a
MPO (U/g)	0.12(0.098)b	0.48(0.147)a
Milk yield (kg)	7.80(0.072)a	7.34(0.177)b

[a–b]Different superscripts within a row denote differences (P<0.05).

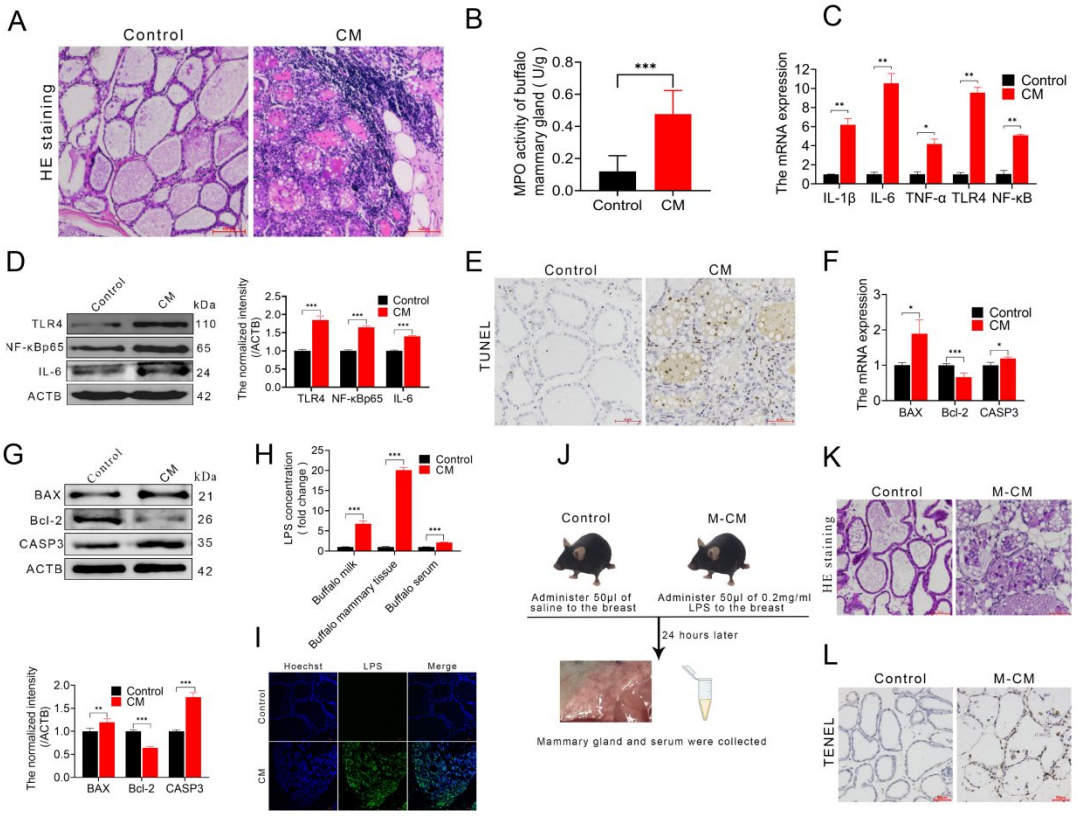

Figure 1 LPS induces inflammatory injury in buffalo mammary tissue

A: H&E staining of buffalo mammary tissue. Scale bar=100 μm. B: Measurement of MPO activity in buffalo mammary tissue. C: qPCR analysis of *IL-1β*, *IL-6*, *TNF-α*, *TLR4*, and *NF-κB* mRNA expression in buffalo mammary tissue. D: Western blot and quantification of TLR4, NF-κBp65, and IL-6 protein levels in buffalo mammary tissue. E: TUNEL staining assessing apoptosis levels in buffalo mammary tissue. Scale bar=100 μm. F: qPCR analysis of *BAX*, *Bcl-2*, and *CASP3* mRNA expression in buffalo mammary tissue. G: Western blot and quantification of BAX, Bcl-2, and

CASP3 protein levels in buffalo mammary tissue. H: Quantification of LPS levels in buffalo milk, mammary tissue, and serum by Limulus Amebocyte Lysate assay. I: Immunohistochemical detection of LPS distribution in buffalo mammary tissue. Scale bar=20 μm. J: Mouse mastitis model established by intramammary injection of LPS. K: H&E staining of mouse mammary tissue. Scale bar=50 μm. L: TUNEL staining assessing apoptosis levels in mouse mammary tissue. Scale bar=50 μm. CM, clinical mastitis in buffaloes; M-CM, LPS-induced clinical mastitis model in mice. Data represent mean±SD, n=6 for buffaloes, n=10 for mice. *: P<0.05; **: P<0.01, ***: P<0.001.

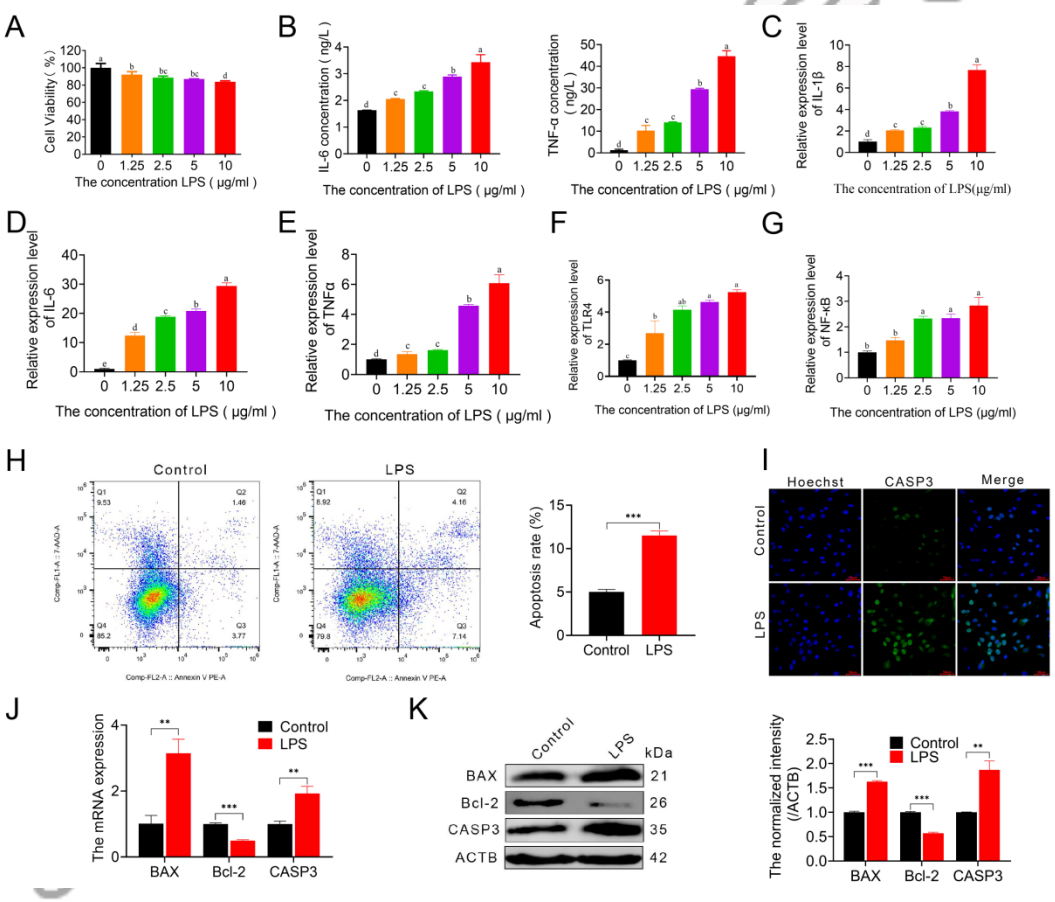

Figure 2 LPS induces inflammation and apoptosis in BuMECs *in vitro*

A: Cell viability of BuMECs after treatment with increasing concentrations of LPS for 12 h. B: ELISA quantification of IL-6 and TNF-α secretion in BuMECs treated with different concentrations of LPS. C: qPCR analysis of *IL-1β* mRNA expression in BuMECs exposed to various LPS concentrations. D: qPCR analysis of *IL-6* mRNA expression in BuMECs exposed to various LPS concentrations. E: qPCR analysis of *TNF-α* mRNA expression in BuMECs exposed to various LPS concentrations. F:

qPCR analysis of *TLR4* mRNA expression in BuMECs exposed to various LPS concentrations. G: qPCR analysis of *NF-κB* mRNA expression in BuMECs exposed to various LPS concentrations. H: Flow cytometry analysis of apoptosis rates in BuMECs. I: CASP3 immunofluorescence staining in BuMECs. Scale bar=50 μm. J: qPCR analysis of *BAX*, *Bcl-2*, and *CASP3* mRNA expression in BuMECs. K: Western blot and quantification of BAX, Bcl-2, and CASP3 protein levels in BuMECs. Data represent mean±SD, n=3 independent experiments. *: P<0.05; **: P<0.01, ***: P<0.001. Different letters indicate significant differences among groups (P<0.05).

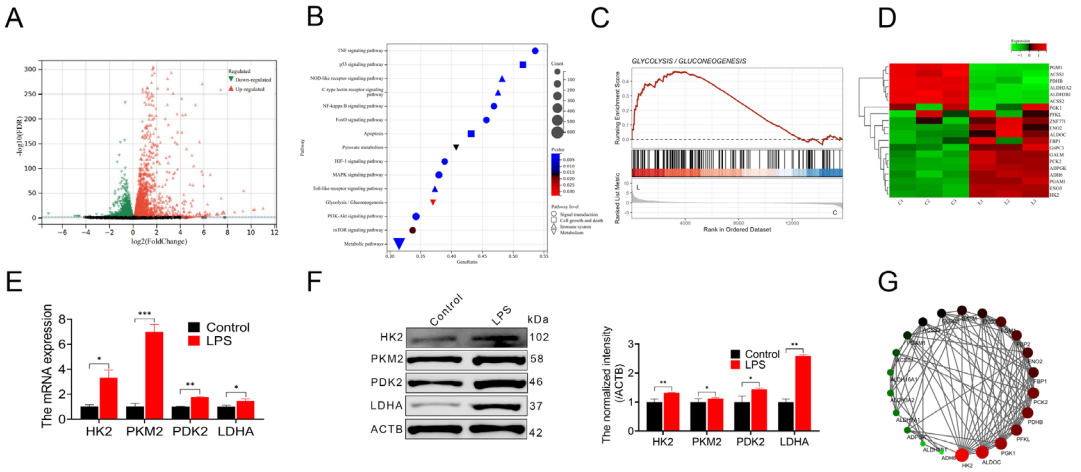

Figure 3 LPS upregulates glycolytic activity in BuMECs

A: Volcano plot of differentially expressed genes between control and LPS-treated BuMECs. B: KEGG pathway enrichment analysis of upregulated genes. C: GSEA analysis of glycolysis/gluconeogenesis pathway. D: Heatmap of glycolysis-related genes showing expression changes. E: qPCR analysis of *HK2*, *PKM2*, *PDK2*, and *LDHA* mRNA expression in BuMECs. F: Western blot and quantification of HK2, PKM2, PDK2, and LDHA protein expression in BuMECs. G: PPI network interaction diagram showing glycolytic enzyme connections. Data represent mean±SD, n=3 independent experiments. *: P<0.05; **: P<0.01, ***: P<0.001.

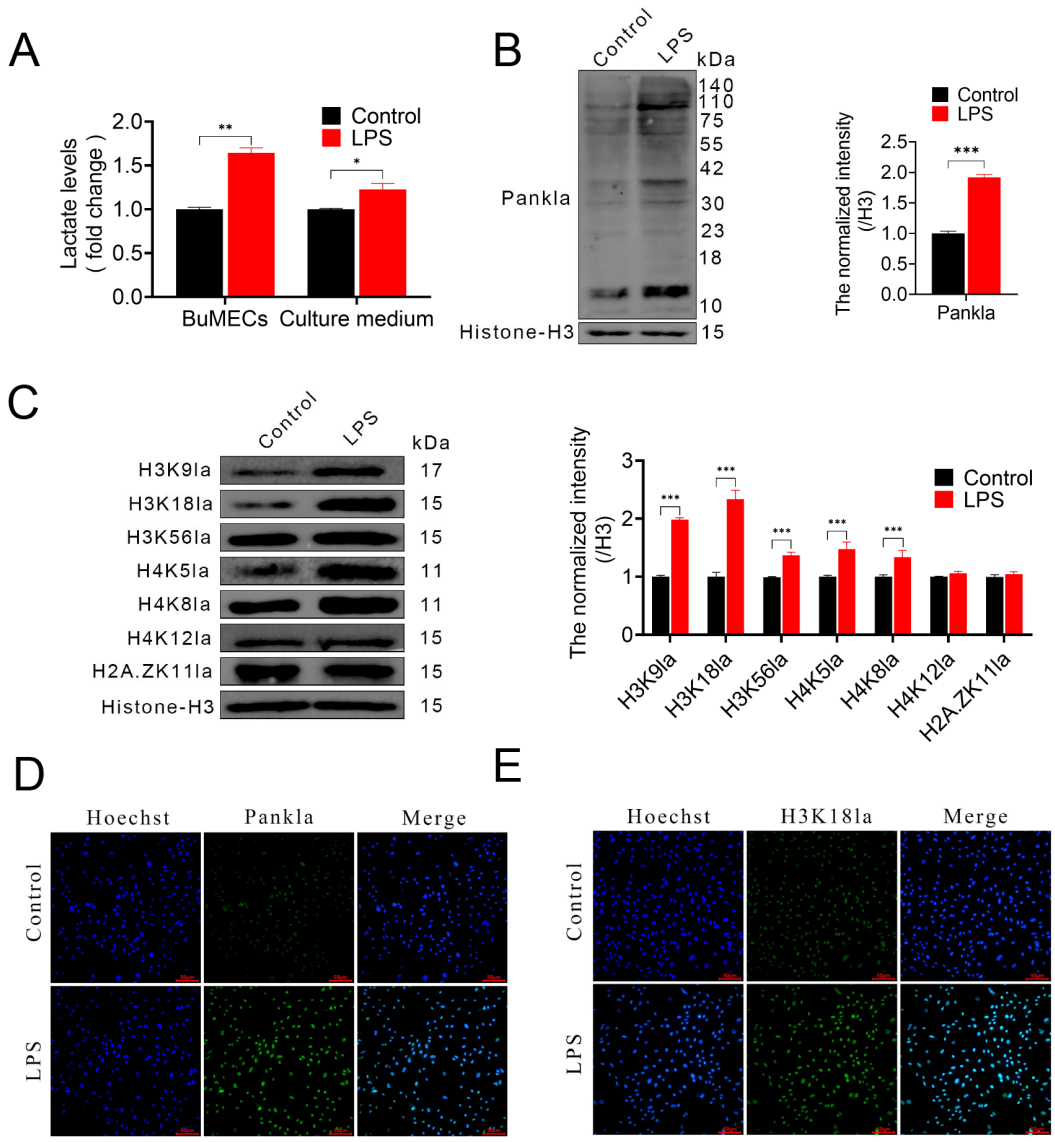

Figure 4 Inflammation leads to lactate accumulation and increased histone lactylation levels in BuMECs

A: Intracellular and extracellular lactate levels in BuMECs measured after LPS treatment. B: Western blot analysis and quantification of PanKla in BuMECs. C: Western blot analysis and quantification of histone lactylation at multiple sites in BuMECs. D: Immunofluorescence staining showing Pankla levels in BuMECs after LPS treatment. D: Immunofluorescence staining showing Pankla levels in BuMECs after LPS treatment.Scale bar=50 μm. E: Immunofluorescence staining and quantification of H3K18la in BuMECs. Scale bar=50 μm. Data represent mean±SD, n=3 independent experiments. *: P<0.05; **: P<0.01, ***: P<0.001.

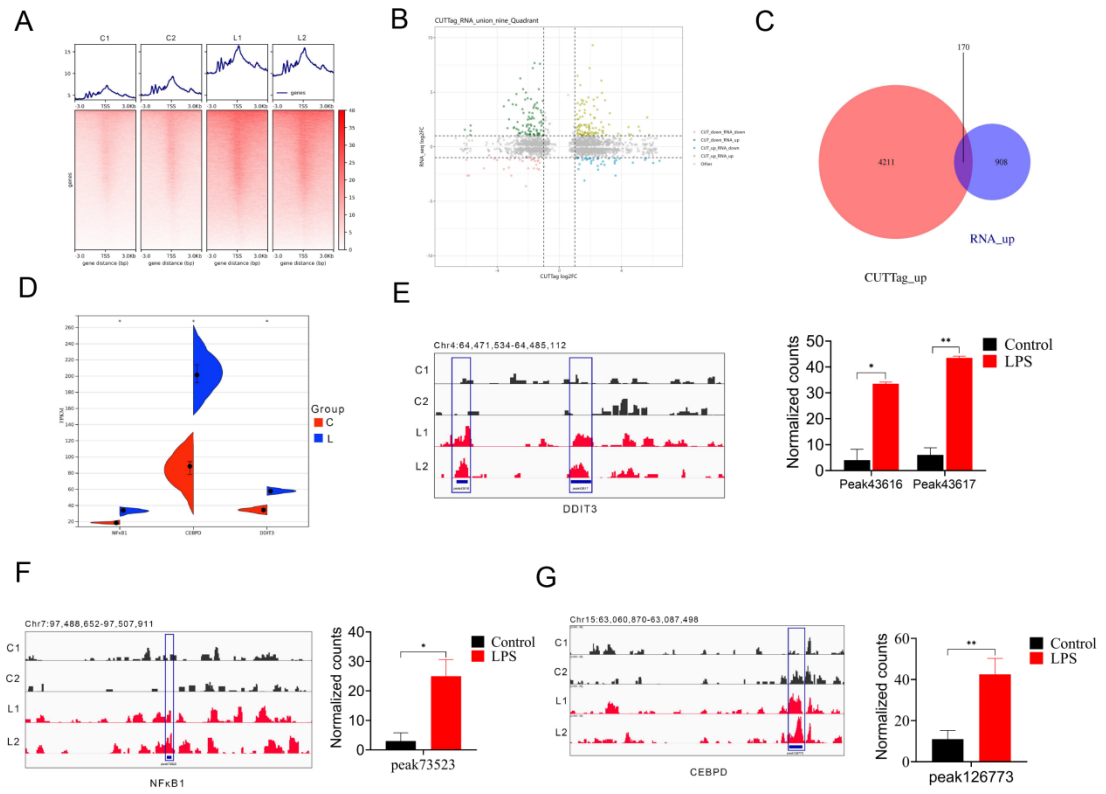

Figure 5 Integrated CUT&Tag and transcriptome analysis identifies key lactylation-regulated genes in LPS-treated BuMECs

A: Heatmap and profile plot showing H3K18la signal distribution across gene regions in control and LPS-treated groups. B: Nine-quadrant scatter plot displaying the relationship between H3K18la peak intensity changes (CUT&Tag) and mRNA expression changes (RNA-seq). Each dot represents a gene. The upper-right quadrant contains genes with both increased H3K18la modification and elevated mRNA expression. C: Venn diagram displaying overlap between upregulated H3K18la peaks (CUT&Tag) and upregulated genes (RNA-seq), identifying 170 candidate genes. D: Violin plot showing transcriptional differences of *NF-κB1*, *DDIT3*, and *CEBPD* between control and LPS groups. E: IGV visualization of H3K18la enrichment at *NF-κB1* promoter region. F: IGV visualization of H3K18la enrichment at *DDIT3* promoter region. G: IGV visualization of H3K18la enrichment at *CEBPD* promoter region. Data represent n=2 biological replicates. *: P<0.05; **: P<0.01, ***: P<0.001.

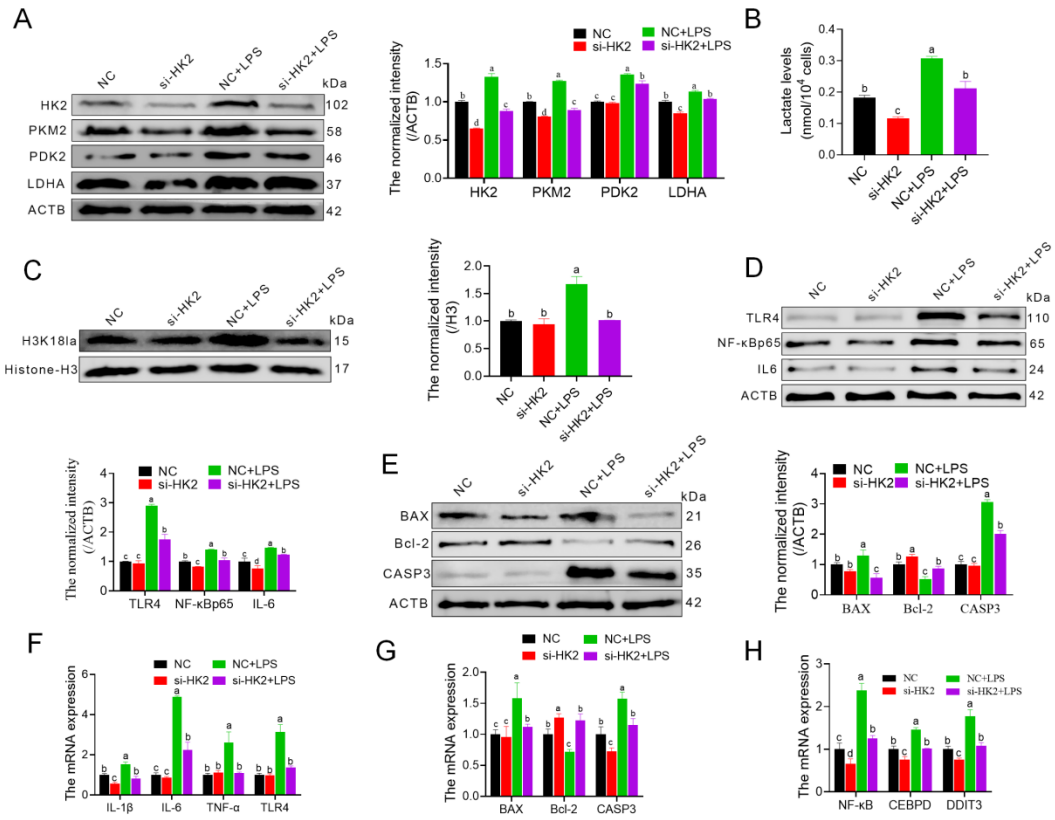

Figure 6 *HK2* knockdown reduces H3K18 lactylation and alleviates inflammatory injury in BuMECs

A: Western blot and quantification of HK2, PKM2, PDK2, and LDHA protein expression in NC, si-HK2, NC+LPS, and si-HK2+LPS groups. B: Intracellular and extracellular lactate levels in BuMECs. C: Western blot and quantification of H3K18la levels. D: Western blot and quantification of TLR4, NF-κBp65, and IL-6 protein expression. E: Western blot and quantification of BAX, Bcl-2, and CASP3 protein expression. F: qPCR analysis of *IL-1β*, *IL-6*, *TNF-α*, and *TLR4* mRNA expression. G: qPCR analysis of *BAX*, *Bcl-2*, and *CASP3* mRNA expression. H: qPCR analysis of *NF-κB1*, *CEBPD*, and *DDIT3* mRNA expression. NC, negative control; si-HK2, HK2 siRNA knockdown. Data represent mean±SD, n=3 independent experiments. Different letters indicate significant differences among groups (P<0.05).

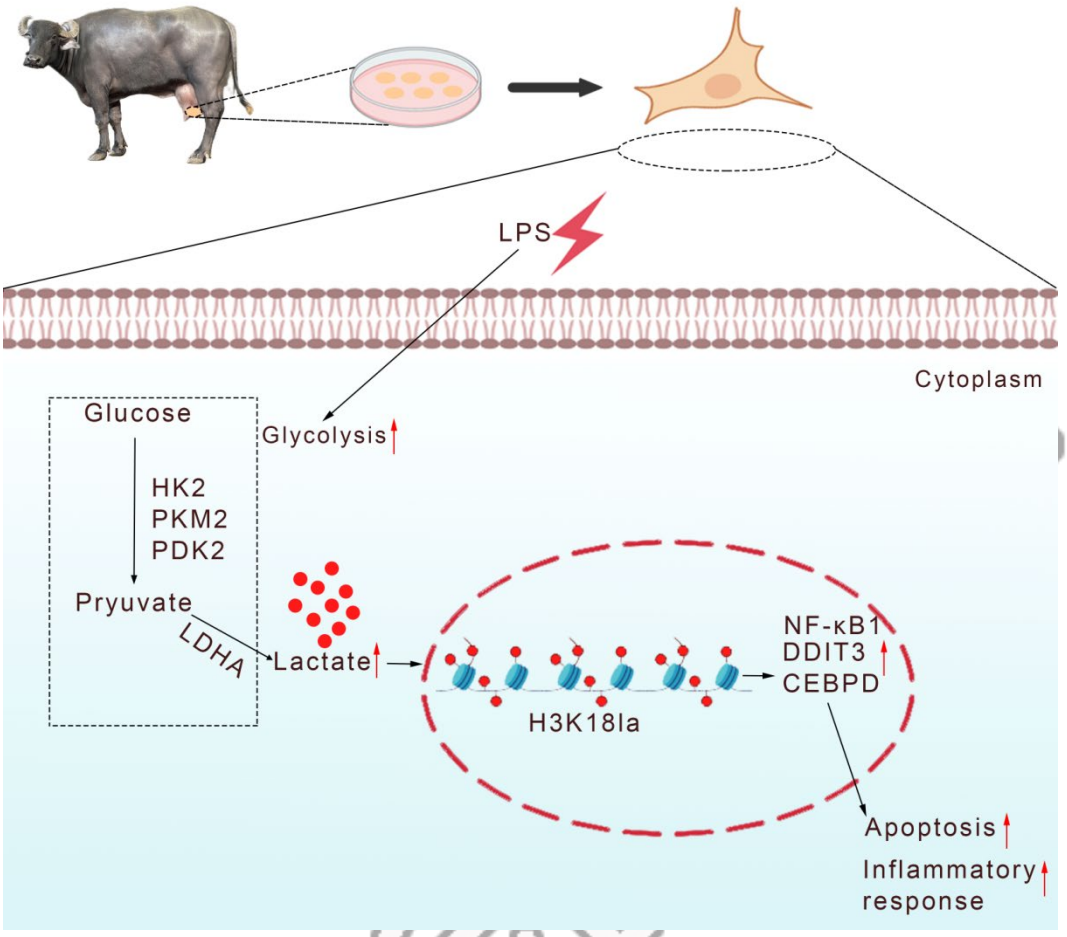

Figure 7 Schematic illustration of the HK2-lactate-H3K18la axis in LPS-induced inflammatory injury in BuMECs

LPS stimulation reprograms cellular metabolism in buffalo mammary epithelial cells by upregulating glycolytic enzymes *HK2*, *PKM2*, *PDK2*, and *LDHA*, leading to intracellular lactate accumulation. Lactate-driven H3K18la at gene promoters facilitates recruitment and activation of transcriptional regulators *NF-κB1*, *DDIT3*, and *CEBPD*, thereby amplifying inflammatory and apoptotic responses in mastitis. *HK2* inhibition attenuates this metabolic-epigenetic cascade, identifying the HK2-lactate-H3K18la axis as a promising therapeutic target.

脂多糖诱导的糖酵解重编程驱动 H3K18 乳酸化介导水牛乳腺上皮细胞炎症损伤

肖鹏[1,2,3,4]，田新如[1,2,3]，周金陈[2,3]，张博[1]，李孟琪[1,2,3]，杨春艳[2,3]，郑海英[2,3]，陈孟姣[4]，杨小淦[1]，尚江华*[2,3]，梁兴伟*[1]

[1]广西大学动物科技学院，广西畜禽繁育与疾病防控重点实验室，南宁 530004

[2]中国农业科学院广西水牛研究所，广西水牛遗传繁殖与育种重点实验室，南宁 530001

[3]中国农业农村部水牛遗传繁育技术重点实验室，南宁 530001

[4]广西农业职业技术大学动物科技学院，南宁 530007

*通讯作者：梁兴伟（邮箱：xwliang@gxu.edu.cn）；尚江华（邮箱：jh_shang@163.com）

摘要：乳房炎会导致水牛产奶量和奶品质下降，但其潜在的表观遗传机制尚不清楚。虽然脂多糖（Lipopolysaccharide，LPS）诱导的糖酵解激活和乳酸积累会导致炎症，但在组蛋白乳酸化介导的炎症损伤中的作用机制尚不明确。本研究结果表明，与健康对照组相比患有临床乳腺炎的水牛乳腺组织中 LPS 水平升高，炎症标志物表达上调，细胞凋亡增强，乳酸、Pankla 和 H3K18la 的水平也显著升高。同样，LPS 诱导的小鼠乳房炎模型重现了水牛组织中观察到的炎症和凋亡特征，证实了 LPS 是乳腺组织损伤的关键驱动因素。体外实验表明，LPS 处理水牛乳腺上皮细胞（Buffalo mammary epithelial cells，BuMECs）可上调促炎和促凋亡标志物，同时下调抗凋亡基因。转录组测序和蛋白质免疫印迹分析进一步揭示，LPS 增强了 *HK2*、*PKM2*、*PDK1* 和 *LDHA* 糖酵解酶的表达活性，从而促进糖酵解通量，增加乳酸生成，并提高 Pankla 和 H3K18la 的水平。CUT&Tag 分析表明，H3K18la 促进 *DDIT3*、*NF-κB1* 和 *CEBPD* 转录调节因子的募集，从而可能将乳酸化与炎症和凋亡通路的激活联系起来。重要的是，*HK2* 抑制剂可减少乳酸积累，降低 H3K18la 水平，并显著减轻 BuMECs 中的炎症损伤。综上所述，本研究表明 HK2-乳酸-H3K18la 轴是 LPS 诱导 BuMECs 炎症损伤的核心作用机制，其作为治疗靶点在缓解水牛乳房炎和改善乳腺健康方面具有潜在价值。

关键词：脂多糖；乳房炎；水牛乳腺上皮细胞；糖酵解；组蛋白乳酸化